


RESEARCH

Open Access



Numerical analysis of laterally loaded barrettes performance in cohesionless soils

Sherif A. Y. Akl¹, Abdelrahman N. Ismail¹, Mahmoud Abdelmoghni^{1,2*}  and Yasser A. Hegazy¹

*Correspondence:
mah.abdelmoghni@engmet.edu.
eg; mah.abdelmoghni@gmail.
com

¹ Soil Mechanics
and Foundations Research
Laboratory, Cairo University, Cairo
University Rd, Giza, Egypt

² Civil Engineering Department,
MISR Higher Institute
for Engineering and Technology,
Mansoura, Egypt

Abstract

This paper investigates the performance of a single and a group of laterally loaded barrettes using a series of numerical models in a three-dimensional finite element software. The simulation of laterally loaded barrettes in both directions is verified by comparing numerical predictions to field measurements previously published in the literature. This paper defines the soil wedge around the barrette sheared at a strain equivalent to the minimum shear strain value at the barrette side or higher as the effective strain wedge. The results from a suite of numerical experiments show that the size of the effective shear strain wedge remains constant at different lateral loads, soil density, barrette shape (aspect ratio), and barrette stiffness. This paper also delineates the effect of spacing in a group of barrettes on the mobilized strain wedges and the associated lateral deformations. The paper then suggests equivalent dimensions for laterally loaded barrettes to be used as input parameters in analyses using p-y curves based on the shape of the effective strain wedge. The predictions from p-y analyses are improved in all the studied cases when equivalent dimensions are used compared to the finite element computations. The paper studies the appropriate design multipliers recommended in literature to be used in the p-y curves method for laterally loaded barrette groups in single and multiple rows. Comparisons with finite element results show the validity of employing the equivalent shape dimensions in determining suitable p-multipliers.

Keywords: Numerical analysis, Barrettes, Strain wedge, Lateral loads, Group action

Introduction

Barrettes are rectangular piles constructed using similar methods like the diaphragm walls drilled by clamshell or hydrofraise machines and stabilized by bentonite or polymers to maintain opening integrity. This type of deep foundations is typically used in projects with special conditions such as extremely large axial loads as in high-rise buildings or when large lateral loads are expected as in offshore structures. For example, barrettes are used in the foundation of the Petronas Towers in Malaysia, the Dubai Creek Tower in the United Arab Emirates [1], the Union Square Tower in Hong Kong, and the Thiam Ruam Mit Station in Thailand. The many advantages of barrettes as deep foundations make it the common choice for high-rise buildings: the possibility of reaching extremely large depths, higher lateral and axial capacities, and more accurate verticality

during construction. Barrettes can be as deep as 100 m and with the same cross-sectional area as a circular pile mobilizes larger friction with surrounding soil leading to higher axial capacity. Higher resistance is attained if the barrette's strong axis is aligned in the expected significant lateral load direction compared to similar circular piles.

The calculation of barrette axial capacity follows similar methodologies to that of the circular piles. However, the high aspect ratio of barrettes makes the lateral capacity considerably different from that of circular piles. Typically, the calculation of circular piles lateral capacity follows the work of Broms [2] using the method of slip lines or the work of Randolph and Houlsby [3] using limit analysis. Several researchers [4–6] concluded that the lateral resistance of the rectangular piles is higher than similar circular piles due to larger shear stresses developing on the sides of the pile when friction with soil is induced. Keawsawasvong and Ukritchon [7] provided a specific solution for the lateral capacity of barrettes using finite element limit analysis. This solution is limited to the full flow failure case at the barrette's deeper depths in a two-dimensional setting.

On the other hand, most design methods depend on predicting the lateral load-displacement curves rather than ultimate lateral capacity. Research relates field test results to barrette lateral deformations [8, 9]. However, the most common method to determine the lateral performance of piles is the p-y curves method. This method considers the soil medium around the pile as discrete springs and assigns a nonlinear relationship between the load on the soil/spring (p) and the soil deformation/spring compression (y) [10]. The p-y curves method has been developed greatly over the years through several studies and a large number of field lateral load tests. Bouzid et al. [11] provided modified p-y curves for designs consistent with the American Petroleum Institute (API) methods. Kim et al. [12] tied p-y functions to results of cone penetration tests (CPT). Kim et al. [13] and Shi et al. [14] discussed how p-y curves could depict the effects of cyclic loading and pile group behavior. The p-y curves method was also incorporated in several commercial software packages such as LPILE [15] and PileLAT [16]. The bulk of the field tests were performed on instrumented circular piles. Hence, the effect of shear between barrette sidewalls and soil imposes limitations on p-y curve predictions.

Further studies on laterally loaded piles, especially those in groups or liquefiable soil conditions, discerned more shortcomings of the p-y curve predictions [17–19]. These studies outlined the importance of studying the mobilized shear strain wedge behind the piles to improve the p-y curve predictions in special conditions. The shear strain wedge is assumed to take the shape of a three-dimensional inverted pyramid. Then, the analysis formulates one-dimensional p-y relationships based on the foundation configuration and the properties of the soil in the wedge. Other studies showed that strain wedges could be conical in softer soils or loose sands [20, 21]. If the strain wedge's shape would depart from the typical case due to loading conditions or pile properties, p-y curve predictions may be inaccurate.

The problem with typical p-y analysis when dealing with lateral loads on pile groups comes from the edge and shadow effects between adjacent piles. These effects decrease the lateral resistance of a pile in a group compared to a single pile performance. As a laterally loaded pile transfers its load to the same soil volume as the one behind it (shadow effect) or beside it (edge effect), the lateral pile displacements relatively increase. Several researchers [18, 22] solved this problem by relating the lateral performance with the

strain wedge mobilized by the group as one continuous body. However, the typical practice uses experience and empirical correlations to develop p-multipliers to account for the shadow and edge effects in the p-y analysis. These methods need to be thoroughly examined in laterally loaded barrettes as the barrette spacings would have a more severe effect on the mobilized shear on the sides.

Another approach to deal with p-y curve limitations is to use equivalent dimensions of the considered deep foundation. Akl et al. [20] proposed equivalent dimensions for helical piles. They suggested the equivalent dimensions based on the mobilized shear strain wedge around the helices in this work. Circular equivalent dimensions have been used before to deal with barrettes under lateral loads using the boundary element-based program CLAP [23].

This paper gives a detailed investigation of the mobilized shear strain wedge around laterally loaded barrettes using three dimensional finite element analyses (3DFE). The numerical setup is validated by comparisons with field tests near the Lai King Subway Station in Hong Kong [9]. The paper then studies the effect of several factors such as lateral load value, soil density, barrette aspect ratio, barrette stiffness, and group spacing and configuration. The paper describes an effective strain wedge, which mobilizes around the barrette. The relative size of this effective wedge does not change significantly with any of the study's factors. The paper also uses the effective strain wedge dimensions to produce equivalent rectangular dimensions to be used in p-y curve analyses. This work delineates the improvement in p-y curve predictions using comparisons with 3DFE results.

Visualizing mobilized strains

Modeling a field test using three-dimensional finite element analysis allows visualizing the shear strains mobilized around laterally loaded barrettes. The chosen field test site is a reclaimed land near the Lai King Subway Station in Hong Kong [9]. The ground level and the groundwater table are +6.5 m and +1.3 m, respectively, above the principal datum. Guide walls were constructed first to guarantee the verticality of the barrette. The tested barrette is 1.2 m wide, 2.7 m deep, and 30 m long. The first 5 m was dug using a clamshell grab, and then, the remainder of the depth was dug using hydrofraise, reverse circulation trench excavation machine. After digging the entire depth, the sides of the opening were scraped, and the bottom was cleaned using the clamshell grab. Two static lateral load tests were performed on the barrette along the major and minor axes. The lateral loading was applied using two hydraulic jacks on opposite sides of the barrette controlling the displacement of the barrette head until it reached a target value. The lateral loads were measured using load cells.

These field tests are simulated using the commercial finite element software Plaxis 3D. In the numerical models, the barrettes are laterally loaded by applying line loads at the side of the barrette top. The magnitude of the line load is incrementally increased until the values measured in the field are reached. There are three major challenges in modeling a laterally loaded barrette in numerical analysis. The first challenge is the computational effort required to build the barrette volume instead of using simpler beam elements. Both the barrette and the surrounding soil are represented by solid tetrahedron elements, which have ten nodes. The second challenge is to calibrate the

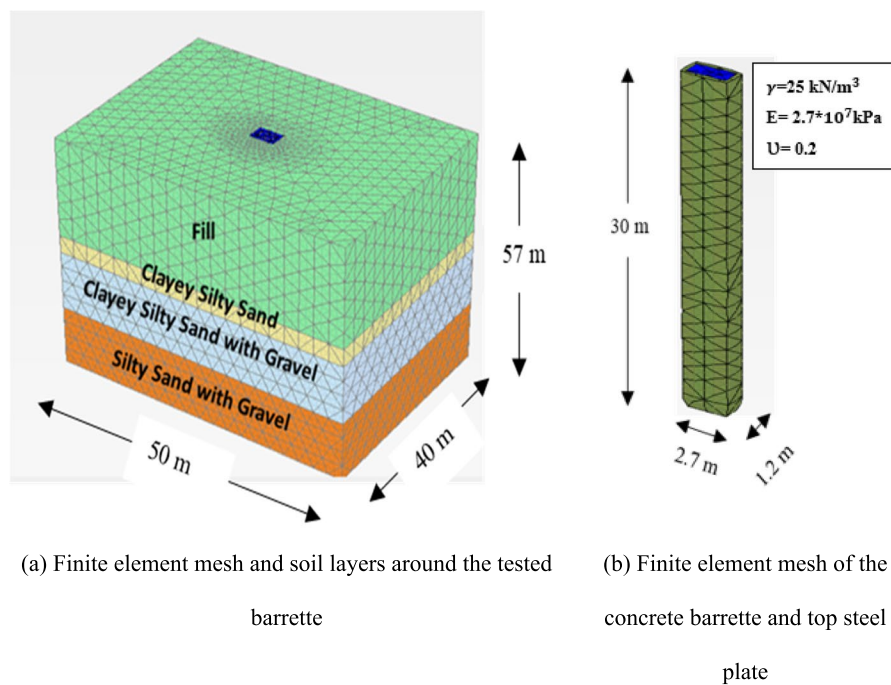


Fig. 1 The finite element mesh adopted in the analysis. **a** Finite element mesh and soil layers around the tested barrette. **b** Finite element mesh of the concrete barrette and top steel plate

Table 1 Stiffness and strength input parameters for simulating the field lateral load test

Depth (m)	Layer	Average (N)	ϕ'	E_h (kN/m ²)	u'
0–17	Fill	21	37°	74,800	0.4
17–20	Clayey silty sand	40	41°	140,000	0.4
20–30	Clayey silty sand with gravel	42	41.5°	145,000	0.4
30–57	Silty sand with gravel	50	44°	186,000	0.4

ratio between the surrounding soil shear parameters (cohesion, friction angle) and the shear parameters describing the friction between the soil and the barrette (“R” value). This value is mostly dependent on method of construction in the absence of very soft layers. This calibration is often based on experience or trial and error. In this analysis, the R value for the interface elements is taken as 0.67. This value often reflects the disturbance in the soil caused by the pile or, in this case, barrette construction [24]. The agreement between computed and measured results shows that $R = 0.67$ is a suitable representation of barrette construction and is used in all the analyses.

Figure 1 shows the finite element model of the field test. The third challenge in this numerical analysis is to define a complete constitutive behavior based on the little information available from site investigation. The mechanical properties of the layers in the model are listed in Table 1. The estimation of friction angle (ϕ') values is based on correlations between the number of blows (N) in the standard penetration test (SPT) and the effective overburden stress according to the Geotechnical Control Office recommendations [25]. The values of horizontal Young’s modulus (E_h) shown in the table are estimated using the Geotechnical Engineering Office practice

recommendations [26] to be within 3000~4000 times the number of blows (kN/m^2). The model uses the simple Mohr-Coulomb constitutive model to represent the soil mechanical behavior to minimize the role of uncertainty in determining the input parameters because only the SPT data is available.

The soil volume extends 25 m in each direction from the center of the barrette along the minor axis, 20 m in each direction from the center of the barrette along the major axis, and 27 m below the barrette tip to minimize the boundary effects on the barrette response. Standard fixities are used such that vertical boundaries are not allowed to deform laterally and the bottom is prevented from movement in all directions. The elements around the barrette make a very fine mesh, which gradually increases in coarseness further away as shown in Fig. 1. The barrette elements are nonporous and assigned a linear elastic behavior with properties of typical concrete material. A horizontal plate cap is added to the top of the barrette head to apply the horizontal loads directly to it. This numerical artifact prevents transversal deformations and transmits the horizontal force uniformly to all the barrette cross-section elements. This plate is relatively very rigid ($E = 1 \times 10^9 \text{ kPa}$). Interface elements are used to represent the soil-barrette interaction and allow slippage between the soil and the barrette. Each interface element consists of six pairs of nodes.

The results from the 3DFE model are compared to the field measurements in Fig. 2. There is a good match between computed deformations and field measurements; however, there is some discrepancy in the unload reload portion. Nevertheless, the numerical model captures the initial slope of the curve and the displacement at the maximum lateral load. The results of the field test in the minor axis also show good agreement with the numerical results. A better validation would have been to compare deformations and straining actions along the depth of the pile. However, it is accepted that the head lateral movements are the results of straining actions and deformations along the pile depth.

Figure 3 shows the distribution of shear strains (γ_s) behind the tested barrette under a lateral load of 800 kN. The FE software visualizes the mobilized strains by computing the distribution of the second invariant of the deviatoric strain tensor in

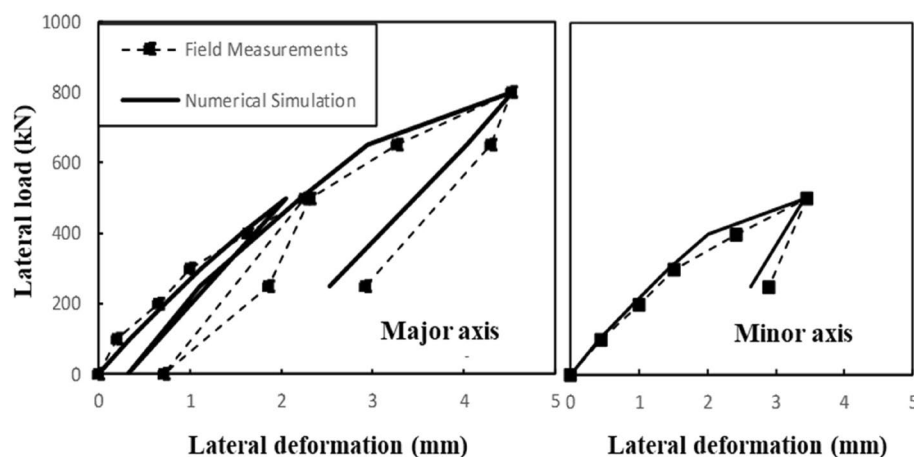


Fig. 2 Computed and measured by Zhang [9] lateral load vs. displacement curves along the major and minor axes

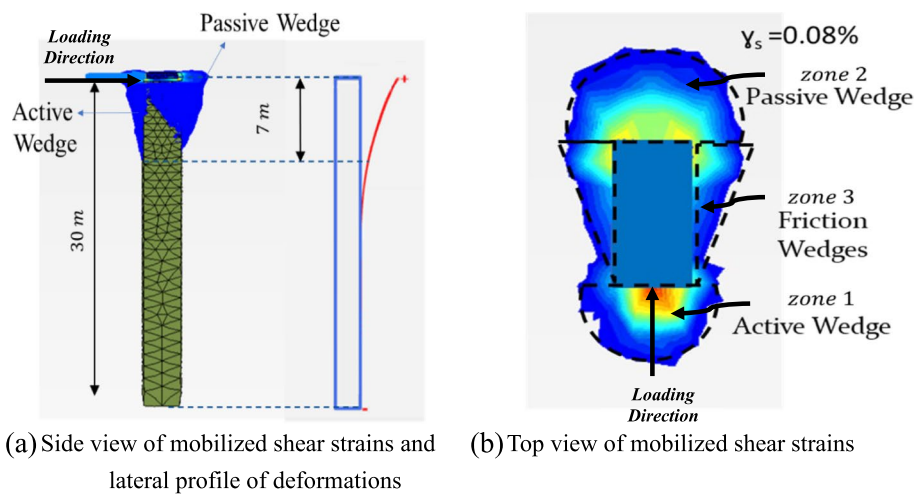


Fig. 3 The shape of the mobilized shear strain. **a** Side view of mobilized shear strains and lateral profile of deformations. **b** Top view of mobilized shear strains

the space around the barrette as described by Akl et al. [20]. The figure also shows the lateral deflection of the barrette (side view) and the ellipsoidal shape of the sheared soil around the barrette (top view). The depth of the significantly strained soil corresponds to the upper deformed part of the barrette. The shear strains around the barrette can be categorized into three different zones, as shown in Fig. 3b. The first zone is the active strain wedge, which is developed due to the gap created by the laterally deforming barrette. The second zone is the passive strain wedge which is directly proportional to the barrette's lateral resistance [17, 18]. There are also significant shear strains at the sides of the barrette (third zone), which develop due to the friction between the laterally moving concrete body and the soil around it. The sheared soil at the sides of the barrette enlarges the passive strain wedge behind the barrette.

Further numerical investigation of the mobilized shear strain wedge around a laterally loaded barrette using a prototype barrette in uniform cohesionless soil is conducted to eliminate the effect of layering on the shape of the wedge. The prototype is 1 m wide (t), 2.5 m deep (d), and 30 m long (L). The stiffness of the prototype barrette is taken as 2.7×10^7 kPa. The lateral loading simulation occurs in loose sand with stiffness taken as $E = 40$ MPa, friction angle, and $\phi = 30^\circ$, and the groundwater table is considered at the ground surface. Figure 4 shows the shear strains around a barrette due to the application of lateral loads equal to 1400 kN, 2400 kN, and 3000 kN. This figure also points to the location where shear strain due to friction between the barrette side and soil is minimal (MSS point). The contour of the shear strain value (γ_s) at MSS envelopes the shaded parts in the shear strain wedge. The shaded parts include a segment from the passive wedge immediately behind the barrette (zone 2) and segments on the sides of the barrette (zone 3). These segments of sheared zones are all encompassed by the same contour line and are called henceforth as the effective strain wedge. Despite the lateral load increase, the dimensions of the effective strain wedge do not appear to change. That wedge is enveloped by a contour of shear

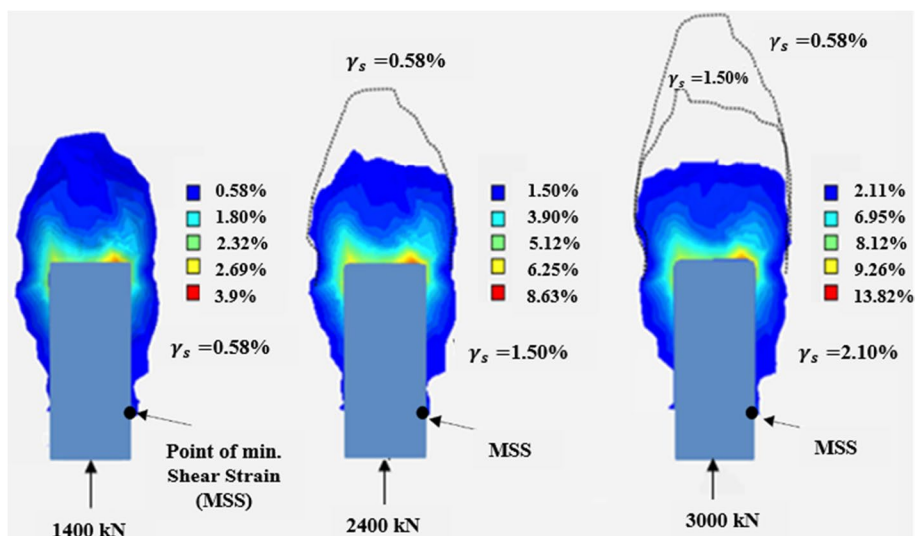


Fig. 4 The shape of effective shear strain wedge behind a laterally loaded barrette with lateral load increase

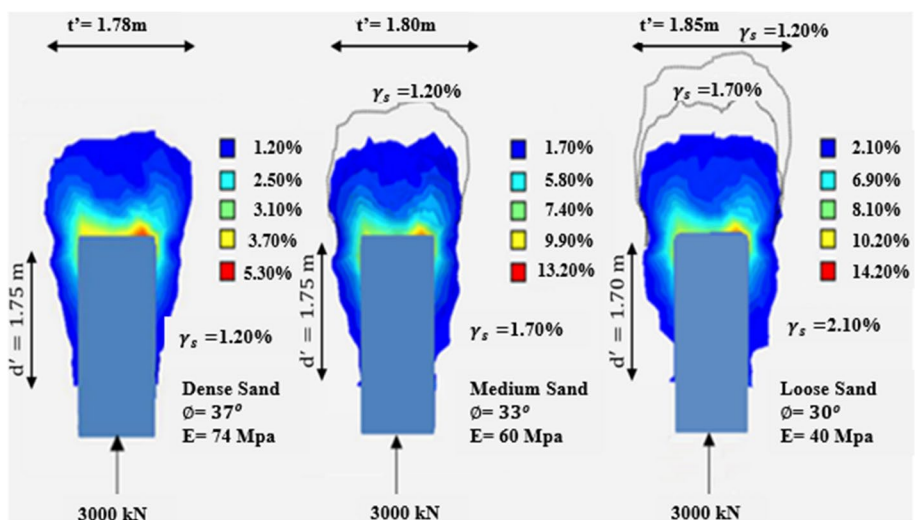


Fig. 5 The effective strain wedge developed behind laterally loaded barrettes in sand soils with different relative densities

strain whose value corresponds to that of the MSS point. The shear strain increases from 0.58 to 1.5% and finally to 2.1% with increasing the lateral load. The size of the new contour line at each load is similar to that of the envelope contour at the previous load; hence, the size of the effective wedge remains approximately constant.

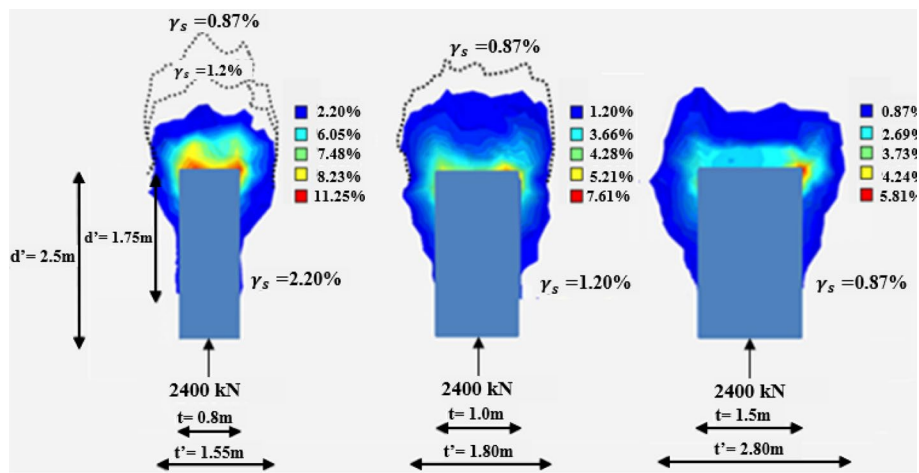
Variation in effective strain wedge

A series of numerical simulations investigate how the shape and size of the effective strain wedge around laterally loaded barrettes change with several factors. These numerical simulations use the same prototype barrette described in the previous section.

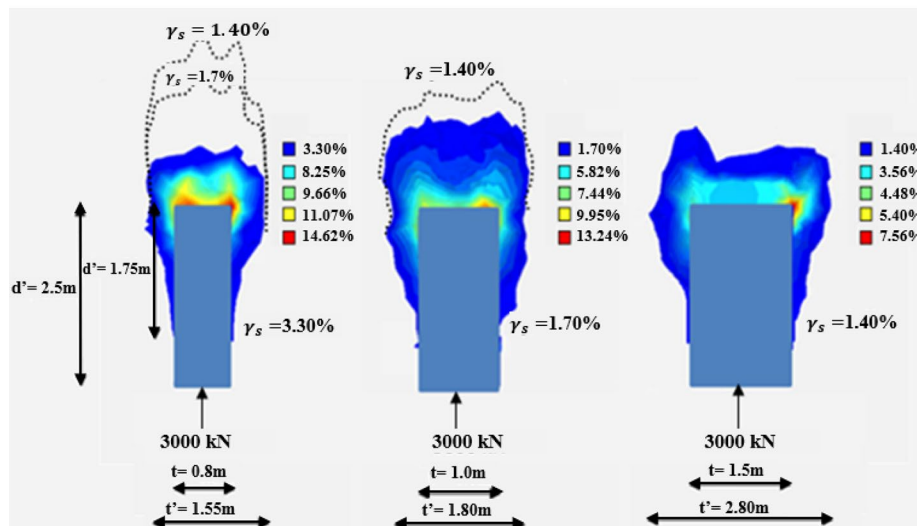
Effect of cohesionless soil relative density

Figure 5 shows the shape of the effective strain wedge around laterally loaded barrettes in sands with different strength and stiffness properties. The figure also lists the chosen parameters representing dense, medium dense, and loose sands. The barrette is loaded laterally along the major axis up to a load of 3000 kN. Despite the variation in shear strain values and sand strength, the effective strain wedge’s shape and size are similar in all three cases.

The MSS point exists at approximately the same location in all simulations where d' ranges from 1.7 to 1.75 m (70% of the barrette depth). The width of the strain wedge, t' , ranges from 1.78 to 1.85 m (1.8 times the barrette width).



(a) Effective strain wedge at lateral load = 2400 kN



(b) Effective strain wedge at lateral load = 3000 kN

Fig. 6 The shape of the effective strain wedge and distribution of shear strains behind laterally loaded barrettes with varying aspect ratios. **a** Effective strain wedge at lateral load = 2400 kN. **b** Effective strain wedge at lateral load = 3000 kN

Effect of barrette aspect ratio

In order to investigate the effect of the barrette aspect ratio, two more barrettes are used in the same numerical setup and following the same methods in medium dense sand with similar properties shown in Fig. 5. A thin barrette is considered with a thickness of 0.8 m, and a thick barrette is considered with a 1.5 m thickness, and both of them are 2.5 m deep. The depth of the barrette is kept constant so that the aspect ratio is 3.125 for the thin barrette and 1.67 for the thick barrette. Figure 6 shows the distribution of shear strains around the barrette at lateral loads 2400 kN (Fig. 6a) and 3000 kN (Fig. 6b) for the three barrettes.

The effective strain wedge is represented in each case by the banded contours (color filled), while lesser strains are shown as contour lines. The size of the effective wedge does not change for each barrette with the lateral loads increase. The value of shear strains inside each effective strain wedge increases with the decrease in barrette thickness. The figure shows that the depth at which the effective wedge develops is constant in all cases (at 70% of the barrette depth). The results show that the ratio of effective wedge width (t') to the barrette width (t) does not deviate much from 1.8. The width of the wedge ranges from 1.55 to 2.8 m. However, the ratio t'/t narrowly ranges from 1.8 to 1.94.

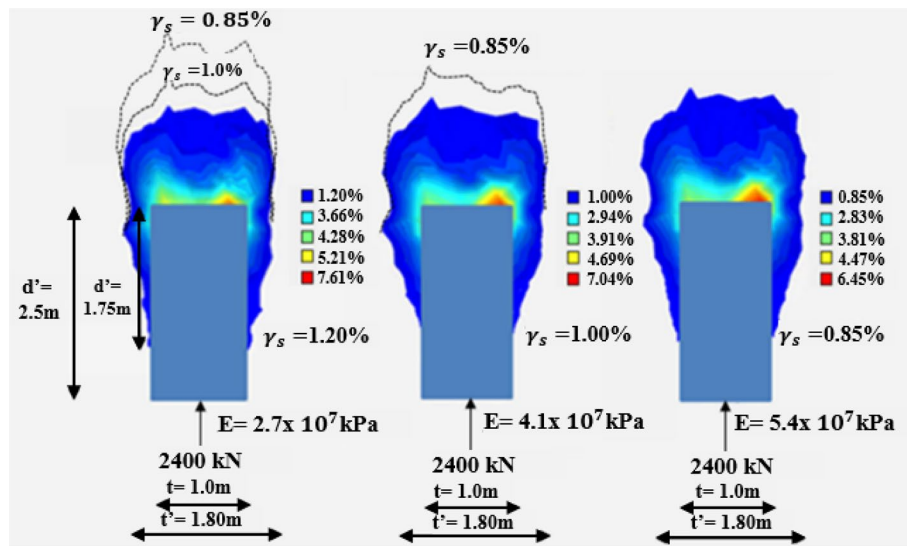
Effect of barrette stiffness

The simulations, shown in Fig. 7, investigate the effect of barrette stiffness on the effective strain wedge. In addition to the prototype barrette stiffness ($E = 2.7 \times 10^7$ kPa), two other barrettes are considered with stiffnesses 1.5 and 2 times the prototype stiffness. The simulations follow similar methods and use similar medium sand properties shown in Fig. 5. The variation in barrette stiffness reflects the possible effect of cracking or special concreting. Figure 7 shows the distribution of shear strains around the barrette at lateral loads 2400 kN and 3000 kN for each stiffness. Despite the decreasing shear strain values with increasing stiffness, the shape and size of the effective strain wedge do not change significantly. The depth at which the MSS point is observed and the width of the wedge are $0.7d$ and $1.8t$ in all cases.

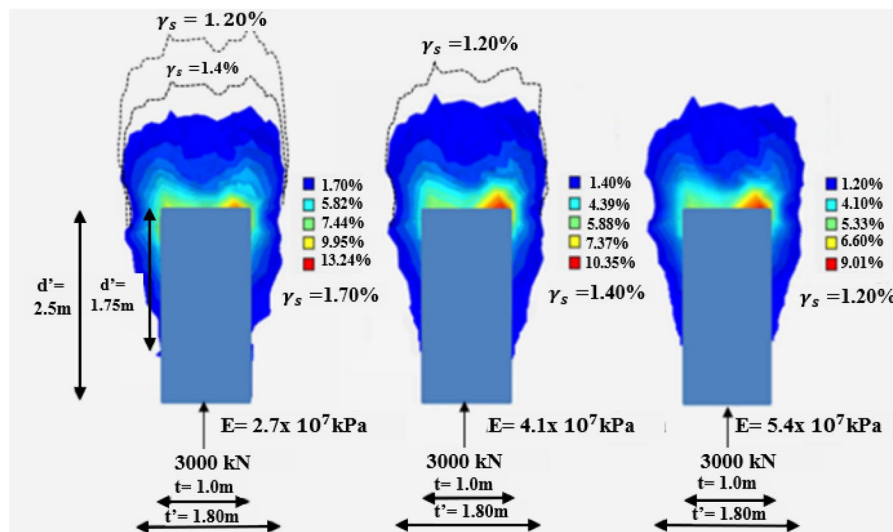
Effect of group action

The expected interference in lateral performance among neighboring barrettes or piles (edge effect) leads to increased lateral deformations compared to a single laterally loaded element. Each barrette affects the soil behind it and the soil behind the barrettes beside it, causing higher displacements at the same lateral load for each barrette. Ashour et al. [18] tied the decrease of the barrette resistance in a group to the interaction between strain wedges behind neighboring piles. Hence, it is expected that barrettes spacing significantly affects its lateral deformations.

A series of numerical models simulate a group of four barrettes in one row with varying spacing to investigate the effect of barrette spacings on effective strain wedge and lateral deformations. The same numerical setup is used as described earlier. Each barrette is 2.5 m deep, 1 m wide, and 30 m long, as shown in Fig. 8. The figure also shows a single numerical model of a 3×4 barrette group to investigate the effect of multiple rows. All



(a) Effective strain wedge at lateral load = 2400 kN

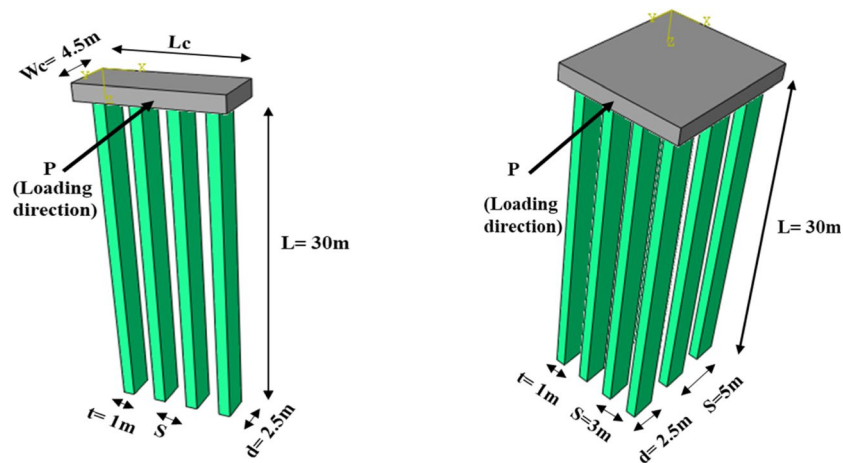


(b) Effective strain wedge at lateral load = 3000 kN

Fig. 7 The shape of the effective strain wedge and distribution of shear strains behind laterally loaded barrettes with varying stiffness. **a** Effective strain wedge at lateral load = 2400 kN. **b** Effective strain wedge at lateral load = 3000 kN

simulations consider the sand around the barrette group to be loose with similar properties to that shown in Fig. 5. The spacing values used are 2t, 3t, 4t, and 5t in the single row group, while the barrettes are spaced at 3t in the multiple row group. A cap of thickness 1.5 m is used to distribute the horizontal force among all the barrettes evenly. The cap width (Wc) and the cap length (Lc) are shown in Fig. 8. This cap is kept above soil level (unlike what usually occurs in real construction) to avoid the effect of soil-cap interaction on the results.

Figure 9 shows the distribution of shear strains around the barrettes in the single row models. Each effective strain wedge is enclosed by a dashed line. The results



(a) One row of barrettes numerical model (b) Three rows of barrettes numerical model

Fig. 8 Configurations of the barrette group models used in 3D finite element simulation. **a** One row of barrettes numerical model. **b** Three rows of barrettes numerical model

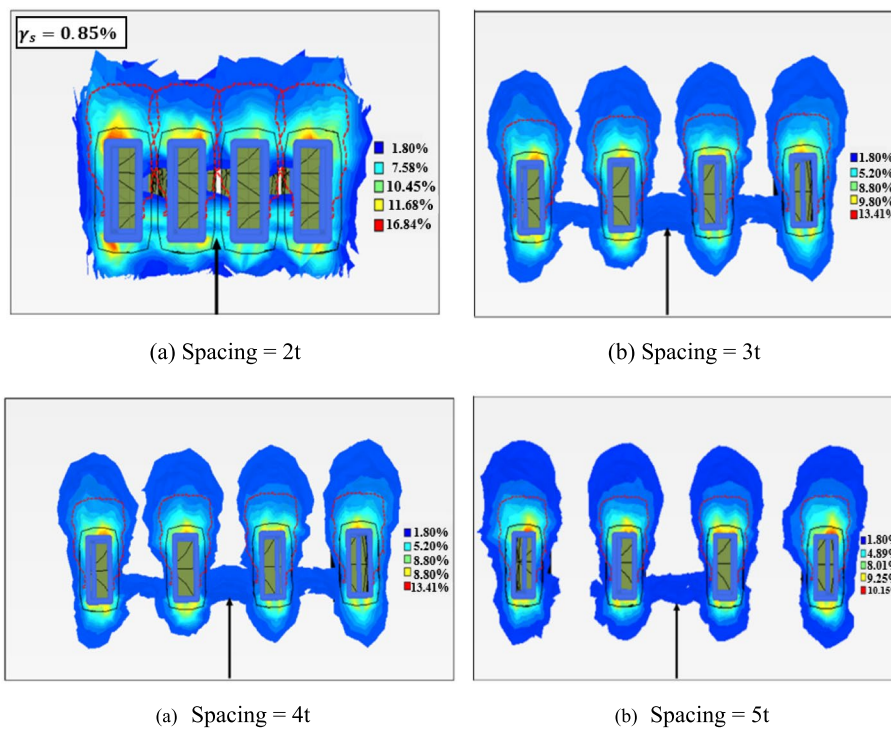


Fig. 9 Distribution of shear strains around one row of laterally loaded barrettes with different spacings. **a** Spacing, 2t. **b** Spacing, 3t. **c** Spacing, 4t. **d** Spacing, 5t

show that the shape of the effective strain wedge is not affected by the barrette spacing. The MSS point is found at $0.7d$ approximately, and the width of the wedge is found to be $1.8t$ in all cases. However, the barrette spacing significantly affects

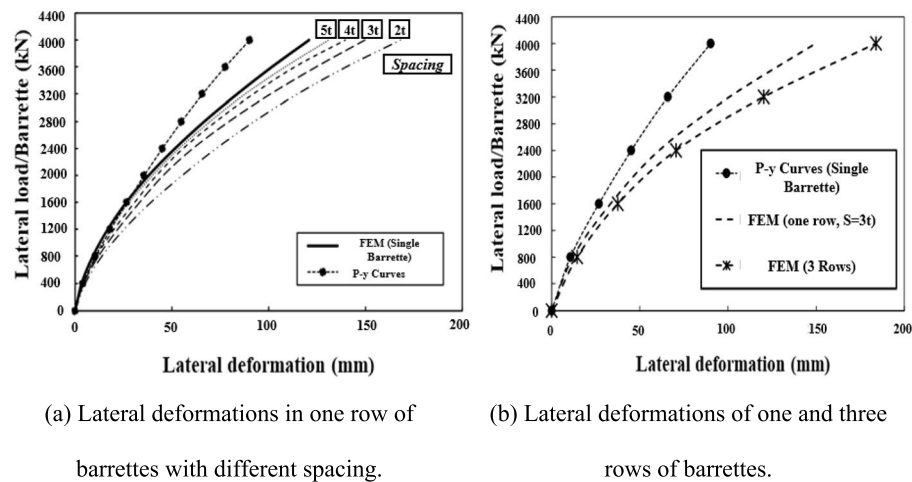


Fig. 10 Comparison between computed deformations between 3DFE models and analysis by p-y curves method. **a** Lateral deformations in one row of barrettes with different spacing. **b** Lateral deformations of one and three rows of barrettes

the computed lateral displacements. Figure 10 shows the lateral load-displacement relationship computed from the analysis of single row models. As a reference, the load-displacement curve from a single barrette is shown from 3D finite elements and computation using the p-y curves method. The larger the spacing, the closer the results to the single barrette case, until the difference is almost negligible at spacing equals 5 times the barrette width. The multiple rows model shows larger deformations than the single row model at the same barrette spacing due to the additional shadow effect. The discrepancy between p-y curves results and 3DFE is aggravated with decreasing the spacing between barrettes in a group.

Applications of effective strain wedge

The simulations in the previous two sections show that there is a noticeable effective strain wedge that develops around the laterally loaded barrette. The dimensions of this wedge do not significantly change with barrette dimensions or stiffness. These dimensions are not affected by barrette spacing in a group or the cohesionless soil density. The width of the wedge is always 1.8 times the width of the barrette, and the minimum shear strains at barrette sides always occur at 0.7 depth of the barrette. An equivalent rectangular section with dimensions $0.7d$ and $1.8t$ would mobilize a similar passive strain wedge observed in numerical analyses. The following subsections investigate the use of equivalent dimensions in improving p-y analysis results. The p-y curve results are computed by different commercial software (LPILE and PileLAT) to guarantee that the conclusions apply to any p-y analysis.

Single barrette performance

Figures 11 and 12 show the lateral load-deflection curves and the lateral load-maximum bending moment curve for the prototype barrette in the three cohesionless soils (cf. Fig. 5). The figures show the results from 3DFE and the p-y curves method. The

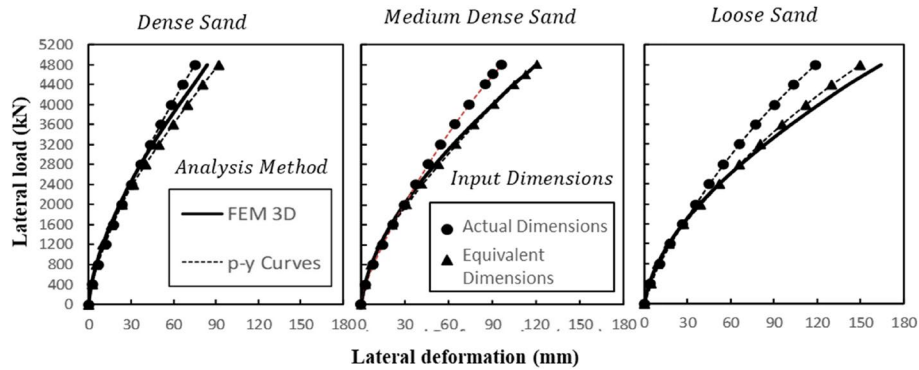


Fig. 11 Computed lateral deformations of barrettes by 3DFE and the p-y curves method using actual and equivalent dimensions

results show that p-y curves overestimate the barrettes’ resistance when the actual dimensions of the cross section are used. The p-y curves predict lower lateral deformations (less conservative in design) and higher bending moments (more conservative in design) at the same lateral load acting on the barrette compared to 3DFE predictions.

A suitable equivalent cross section to the barrette can be taken as $1.8t \times 0.7d$, as shown in Figs. 11 and 12, based on the effective strain wedge observations. The cross-sectional area and moment of inertia are calculated using the equivalent dimensions. Hence, these equivalent dimensions are only used to adjust lateral performance predictions and are not used in predicting axial capacity, and the goal of using the equivalent cross section is not to validate it as it is not considered as a scientific concept but to be used as a numerical trick to help the practitioner engineers rather than using 3D FEM which requires more effort and time. When the equivalent dimensions are used, p-y curve predictions are a lot closer to those of 3DFE and this matching in results as this equivalent area takes the mobilized wedges on the barrettes sides into considerations, so it generates wedge close to what we find in the finite element. In the load-deformation curves, the dense sand results do not show significant differences between p-y curves and 3DFE, whether the equivalent or the

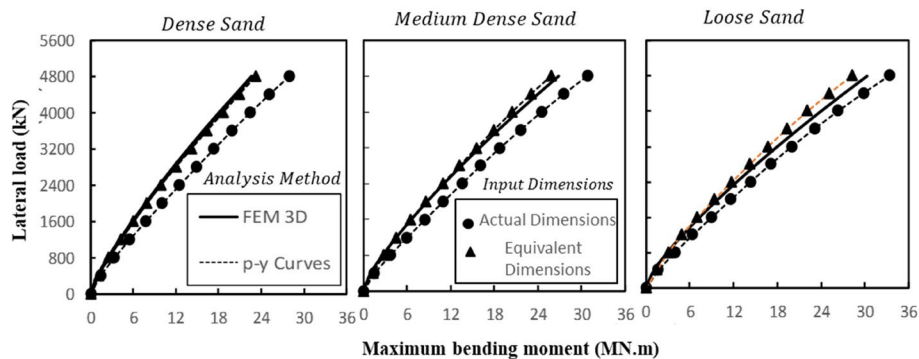


Fig. 12 Computed bending moments in barrettes by 3DFE and the p-y curves method using actual and equivalent dimensions

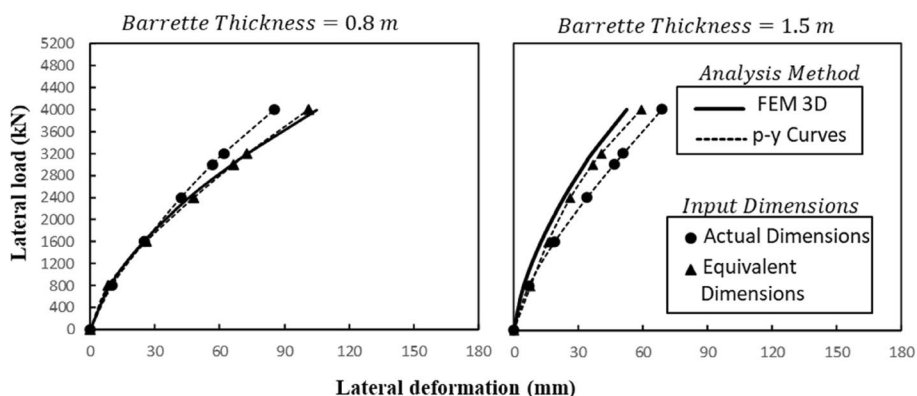


Fig. 13 Computed lateral deformations by 3DFE and the p-y curves method using actual and equivalent dimensions at different barrette thicknesses

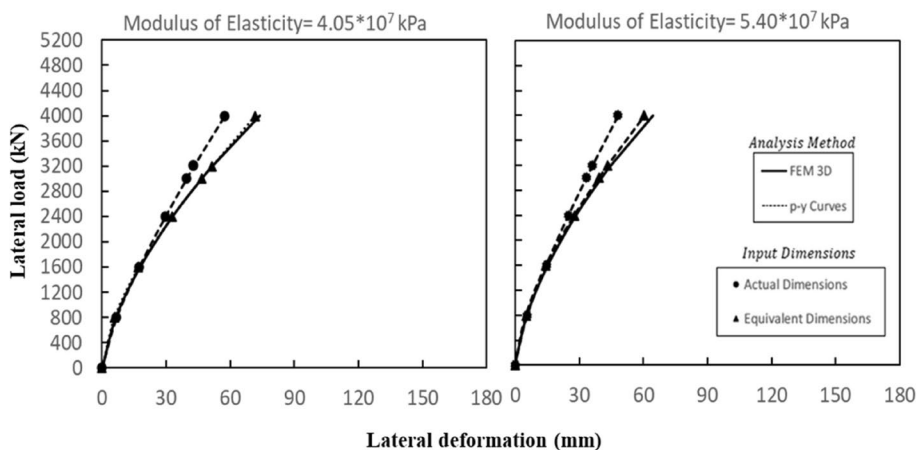


Fig. 14 Computed lateral deformations by 3DFE and the p-y curves method using actual and equivalent dimensions at different barrette stiffnesses

original shapes are used. However, results in loose sand and medium dense sand show significant improvement in p-y curve predictions. In the load-bending moment curves, using the equivalent dimensions produces closer predictions to 3DFE results in all three soils.

Figure 13 shows the lateral load-deformation curves for the thin and thick barrettes (cf. Fig. 6). The curves are computed by 3DFE as well as p-y curves using the original and modified dimensions. When the original dimensions are used, p-y curve predictions are less conservative for the thin barrette and more conservative for the thick barrette. Using the modified dimensions improves p-y curves predictions as compared to 3DFE results. Figure 14 makes the same comparisons for barrettes with higher stiffness values (cf. Fig. 7). The p-y curve predictions are less conservative, but the use of equivalent dimensions in p-y analyses improves predictions compared to 3DFE results.

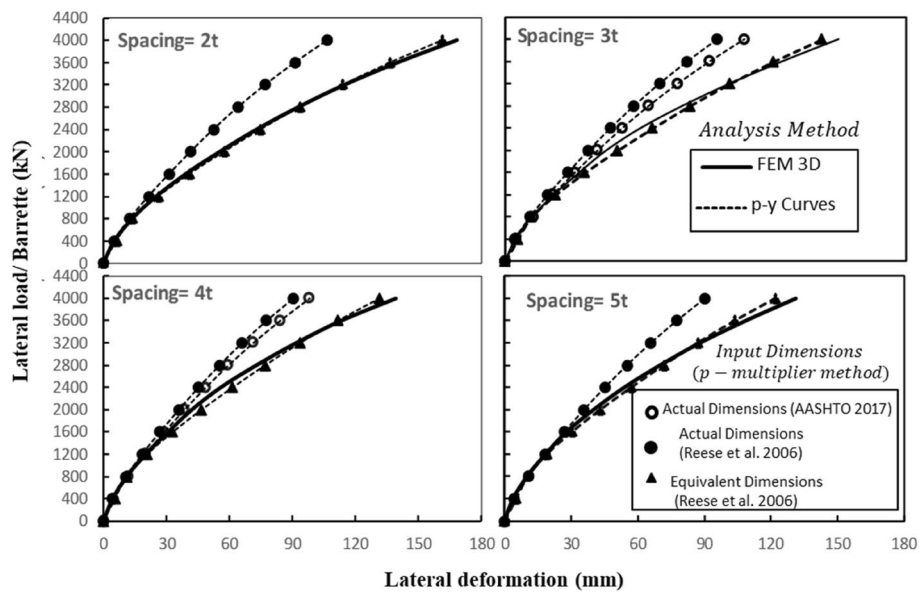


Fig. 15 Computed lateral deformations of one row of barrettes by 3DFE and the p-y curves method using actual and equivalent dimensions to compute p-multipliers

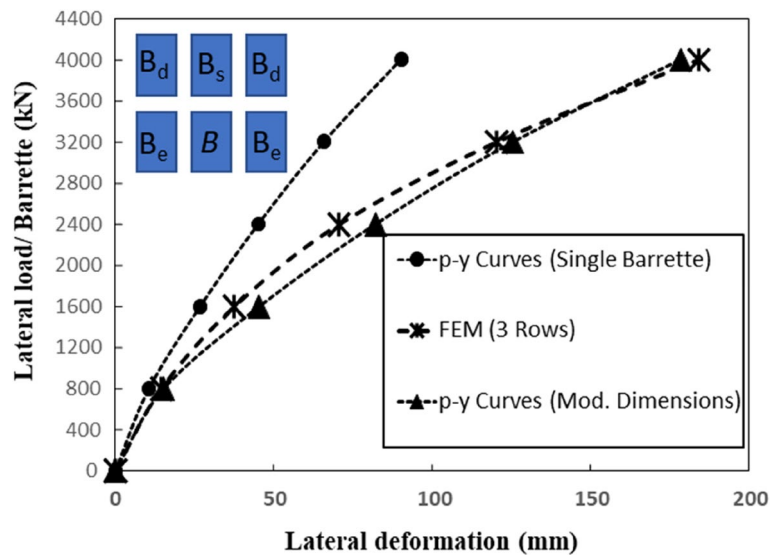


Fig. 16 Computed lateral deformations of a 3 × 4 group of barrettes by 3DFE and the p-y curves method using actual and equivalent dimensions to compute p-multipliers

Appropriate p-multipliers

When p-y curves are used to analyze the lateral performance of pile groups, p-multipliers are typically used to compensate for the edge and shadow effects. Several suggestions for p-multipliers are available in the literature [27, 28]. However, these suggestions are based on observations from cases of loading on typical circular piles. Since the equivalent section concept is based on the resulting strain wedge shape, this concept should be applied to a barrette in a group. AASHTO [27] recommends p-multiplier values of 0.8

and 1 for piles at spacing 3 t and 5 t , respectively. Piles at spacing 4 t may use a p-multiplier value of 0.9 using interpolation. Reese et al. [28] recommend the use of the formula: $P_m = 0.64 (S/t)^{0.34}$ to calculate p-multiplier (P_m) for piles at spacing less than 3.75 times the pile width. Hence, the P_m values are 0.81, 0.93, and 1 for spacing 2 t , 3 t , and 4 t , respectively. Figure 15 shows that when the P_m values suggested by AASHTO [27] or Reese et al. [28] are used, the p-y curve predictions still disagree with the 3DFE predictions and produce less conservative predictions of pile performance.

The equivalent cross-section approach is applied using the modified dimensions ($d' = 0.7 d$, and $t' = 1.8 t$) as input parameters in p-y analysis and the Reese et al. [28] equation to calculate P_m . Hence, P_m values are 0.67, 0.77, 0.84, and 0.91 for barrette spacing 2 t , 3 t , 4 t , and 5 t . Figure 15 shows the results from p-y curves when the equivalent cross section is applied and those curves agree better with 3DFE results.

For multiple rows, Reese et al. [28] gave a detailed method to calculate P_m considering the effect of adjacent piles, piles behind, and the next piles on a diagonal axis. Figure 16 shows the configuration of barrettes considered when p-multipliers are calculated to adjust p-y curves predictions. According to Reese et al. [28], the lateral displacements of the barrette B are adjusted two times for B_e barrettes (adjacent barrettes) by $P_m = 0.93$, one time for B_s barrette (barrettes behind) by $P_m = 0.84$, and two times for B_d barrettes (barrettes on a diagonal axis) by $P_m = 0.86$. If the same methodology of calculating P_m values is followed but using the equivalent dimensions ($0.7d \times 1.8t$), the multipliers become 0.76, 0.91, and 0.87 for the adjacent, behind, and diagonal barrettes, respectively. The adjusted p-y curves prediction is also improved relative to 3DFE results, as shown in Fig. 16.

Conclusions

The passive shear strains mobilized by a laterally loaded barrette are affected by the friction between the barrette sides and the surrounding soil. The paper investigates these shear strains using 3D finite element analysis. The finite element models are validated by comparison with independently published field test results. The shear strain visualization depicts the increasing strain wedge behind the barrette with increasing lateral load. However, a portion of this wedge, which comprises sheared soil at strains equivalent to the minimum shear strains at barrette sides (MSS), has an approximately constant size and is called the effective strain wedge. Different factors affect the value of shear strain at MSS point and the size of the mobilized strain wedge but do not affect the size of the corresponding effective strain wedge. The following are the detailed conclusions:

- The point at which minimum shear strain (MSS point) occurs at the sides of the barrette is approximately located at 70% of the barrette depth in all the considered cases. The effective strain wedge corresponding to MSS has an approximate width equals 1.8 times the barrette width in loose, medium, or dense sands. This width is not affected by the barrette thickness or stiffness.
- The shear strains behind laterally loaded barrettes tend to overlap at spacing between 3 and 4 times the barrette thickness (3~4 t); however, the shape and size of the effective strain wedge remain unchanged even at the improbable low spacing of 2 t .

- Design of deep foundations using the popular p-y analysis approach needs to address the complex shear strain mobilized behind barrettes. An equivalent shape for the barrette can be used as input in p-y analyses. The equivalent shape dimensions are $0.7d$ in depth and $1.8t$ in width, which correspond to the effective strain wedge shape. Results using p-y curves and equivalent dimensions agree with 3DFE results in all the considered cases using any p-y analysis software.
- Two cases of barrette groups are considered: a single row of barrettes and a 3×4 barrette configuration. The p-multipliers suggested in the literature to improve p-y curve predictions for pile groups do not compare well with 3DFE simulation results. Using equivalent dimensions when calculating the p-multipliers improves predictions of p-y analyses.

Abbreviations

p	Load on the soil/spring
y	Soil deformation/spring compression
CPT	Cone penetration test
3DFE	Three-dimensional finite element analysis
R	Ratio between the surrounding soil shear parameters (cohesion, friction angle) and the shear parameters describing the friction between the soil and the barrette
ϕ'	Friction angle
N	Number of blows
SPT	Standard penetration test
E_h	Horizontal Young's modulus
E	Young's modulus
γ_s	Shear strains
t	Barrette wide
d	Barrette deep
L	Barrette long
MSS point	The point at which minimum shear strain
u'	Poisson's ratio
t'	The effective wedge width
Wc	The cap width
Lc	The cap length
S	Barrettes spacing
P_m	P-multiplier
d'	Modified barrette depth
B	Lateral displacements of the barrette
B_e	Adjacent barrettes
B_d	Barrettes on a diagonal axis
B_s	Barrettes behind

Acknowledgements

Not applicable.

Authors' contributions

SAYA suggested the concept and the methodology of this paper and has the main role in writing, editing, and revision of the manuscript. ANI performed the software analyses and validation. MA helped in writing, editing, and revision of the manuscript. YAH reviewed and edited the manuscript. All authors read and approved the final manuscript.

Funding

This research received no external funding.

Availability of data and materials

Data will be made available on request.

Declarations

Competing interests

The authors declare that they have no competing interests.

Received: 22 February 2023 Accepted: 8 May 2023

Published online: 20 May 2023

References

1. Pereira G, Quet FR, Vorster TEB, Wojtowicz G (2019) Overview of the dual foundation system of the Dubai Creek Tower. Proc 17th Eur Conf Soil Mech Geotech Eng. ISSMGE, Reykjavik
2. Broms BB (1964) Lateral resistance of piles in cohesionless soils. *J Soil Mech Found Div* 90(3):123–156
3. Randolph MF, Houlsby GT (1984) The limiting pressure on a circular pile loaded laterally in cohesive soil. *Geotech* 34(4):613–623. <https://doi.org/10.1680/geot.1984.34.4.613>
4. Briaud JL, Smith T, Meyer B (1984) Laterally loaded piles and the pressuremeter: comparison of existing methods. Texas, Texas Transp Institute
5. Smith TD (1987) Friction mobilization F-Y curves for laterally loaded piles from the pressuremeter. Proc an Int Symp Predict Perform Geotech Eng. Calgary, A.A. Balkema, Rotterdam
6. Reese LC, Van Impe WF (2010) Single piles and pile groups under lateral loading, 2nd edn. CRC Press, Boca Raton
7. Keawsawasvong S, Ukritchon B (2016) Ultimate lateral capacity of two dimensional plane strain rectangular pile in clay. *Geomech Eng* 11(2):235–52. <https://doi.org/10.12989/gae.2016.11.2.235>
8. Plumbridge GD, Sze JWC, Tham TTF (2000) Full-scale lateral load tests on bored piles and a barrette. Proc 19th Annu Semin Geotech Eng. ISSMGE, Hong Kong
9. Zhang LM (2003) Behavior of laterally loaded large-section barrettes. *J Geotech Geoenviron Eng* 129(7):639–648. [https://doi.org/10.1061/\(ASCE\)1090-0241\(2003\)129:7\(639\)](https://doi.org/10.1061/(ASCE)1090-0241(2003)129:7(639))
10. Matlock H, Reese LC (1960) Generalized solutions for laterally loaded piles. *J Soil Mech Found Div* 86(5):63–91
11. Bouzid DA, Bhattacharya S, Dash SR (2013) Winkler springs (py curves) for pile design from stress-strain of soils: FE assessment of scaling coefficients using the mobilized strength design concept. *Geomech Eng* 5(5):379–399. <https://doi.org/10.12989/gae.2013.5.5.379>
12. Kim G, Park D, Kyung D, Lee J (2014) CPT-based lateral displacement analysis using py method for offshore monopiles in clays. *Geomech Eng* 7(4):459–475. <https://doi.org/10.12989/gae.2014.7.4.459>
13. Kim G, Kyung D, Park D, Lee J (2015) CPT-based py analysis for mono-piles in sands under static and cyclic loading conditions. *Geomech Eng* 9(3):313–328
14. Shi J, Zhang Y, Chen L, Fu Z (2018) Response of a laterally loaded pile group due to cyclic loading in clay. *Geomech Eng* 16(5):463–469. <https://doi.org/10.12989/gae.2018.16.5.463>
15. Reese LC, Wang ST, Isenhowe WM, Arrellaga JA (2000) LPile Plus 50. Ensoft, Austin
16. PileLAT, (2018) User manual for PileLAT. Innov Geotech Pty, Brisbane
17. Ashour M, Norris G, Pilling P (1998) Lateral loading of a pile in layered soil using the strain wedge model. *J Geotech Geoenviron Eng* 124(4):303–315. [https://doi.org/10.1061/\(ASCE\)1090-0241\(1998\)124:4\(303\)](https://doi.org/10.1061/(ASCE)1090-0241(1998)124:4(303))
18. Ashour M, Norris G, Singh JP (2002) Calibration of strain wedge model predicted response for piles/shafts in liquefied sand at treasure island and cooper river bridge. Proc. of the Third National Seismic Conf. and Workshop on Bridges and Highways, MCEER
19. Ashour M, Norris G (2004) Strain wedge model for piles/shafts in liquefied soil. GeoTrans, Los Angeles
20. Akl SAY, Elhami OM, Abu-Keifa MA (2016) Investigation of the mobilized strain wedge by laterally loaded helical piles. *J Eng Appl Sci* 63(1):39–59. <https://doi.org/10.13140/RG.2.2.15309.74728>
21. Hajjalilue-Bonab M, Sojoudi Y, Puppala AJ (2011) Study of strain wedge parameters for laterally loaded piles. *Int J Geomech* 13(2):143–152. [https://doi.org/10.1061/\(ASCE\)GM.1943-5622.0000186](https://doi.org/10.1061/(ASCE)GM.1943-5622.0000186)
22. Rollins KM, Lane JD, Gerber TM (2005) Measured and computed lateral response of a pile group in sand. *J Geotech Geoenviron Eng* 131(1):103–114. [https://doi.org/10.1061/\(ASCE\)1090-0241\(2005\)131:1\(103\)](https://doi.org/10.1061/(ASCE)1090-0241(2005)131:1(103))
23. Poulos HG, Chow HSW, Small JC (2019) The use of equivalent circular piles to model the behaviour of rectangular barrette foundations. *Geotech Eng J SEAGS AGSSEA* 50(3):106–109
24. Akl SAY, Elhami OM, Abu-keifa MA (2016) Lateral performance of helical piles as foundations for offshore wind farms. Geo-Chicago, Chicago
25. GCO (2017) Guide to retaining wall design. Geotech Control Off Kowloon, Hong Kong
26. GEO (2006) Pile design and construction. Geotech Eng Off Kowloon, Hong Kong
27. AASHTO (2017) LRFD Bridge Design Specifications, 8th edn. American Association of State Highway and Transportation Officials, NW, Washington, USA. LRFD Bridg Des Specif (8th Ed Am Assoc State Highw Transp Off NW. Washington
28. Reese LC, Isenhowe WM, Wang ST (2006) Analysis and design of shallow and deep foundations. Wiley, Hoboken

Publisher's Note

Springer Nature remains neutral with regard to jurisdictional claims in published maps and institutional affiliations.